

Performance enhancement of Sn–Sb–Co alloy film anode for lithium-ion batteries via post electro-dissolution treatment

Xin-Jing Pang · Chun-Hui Tan · Xiao-Hui Dai ·
Xin Wang · Gong-Wei Qi · Shu-Yong Zhang

Received: 13 August 2014 / Accepted: 1 December 2014 / Published online: 6 December 2014
© Springer Science+Business Media Dordrecht 2014

Abstract Sn–Sb–Co alloy films prepared via co-electroplating and post-electrodissolution treatment were studied as anode materials for lithium-ion batteries. The alloy was composed of pure Sn, Sn–Sb, and Sn–Co alloy phases. During post-electrodissolution, the easy dissolution of Sn phase resulted in an increase in Sb and Co contents. Electrochemical measurements showed improved initial capacity and capacity retention with increasing electro-dissolution treatment time. For the sample subjected to 10 min of electro-dissolution treatment, the capacity remained at 580 mAh g⁻¹ at the 50th cycle. Post-electrodissolution was proven to be an effective method to improve the electrochemical performance of ternary Sn-based alloys.

Keywords Lithium-ion battery · Anode material · Sn–Sb–Co alloy · Electro-dissolution treatment · Electrochemical performance

1 Introduction

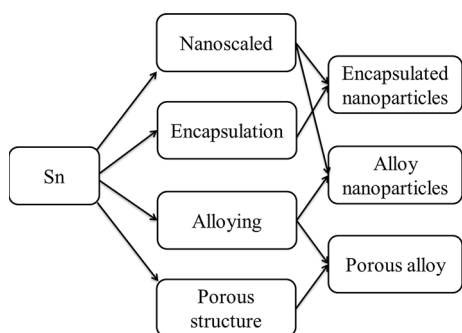
Anodes based on carbonaceous materials with a theoretical capacity of only 372 mAh g⁻¹ cannot meet the requirements of high-energy density lithium-ion batteries (LIBs) for future applications [1]. In the past decades, substantial

efforts have been focused on discovering new materials with high lithium intercalation capacity for LIB applications. Given their high theoretical capacities, Sn, Sb, Si, and Ge have attracted the interest of numerous researchers [2]. Among these metals, Sn-based materials became the most advantageous alternatives for carbonaceous materials because of its higher theoretical capacity (993 mAh g⁻¹) and because it is easier to prepare, less toxic, cheaper, and has more diverse morphologies [1–3]. However, the volume change in pure Sn phase during charge–discharge cycling is as high as 300 %. This large volume expansion leads to serious pulverization of Sn materials and the loss of electric contact of Sn active materials with the current collector, which results in rapid capacity decay, typically in 20–30 cycles [4–6]. To solve this problem, a number of methods have been proposed, as demonstrated in Scheme 1.

One method involves reducing the size of Sn particles. For example, Yu et al. [7] found that nanoscale Sn particles performed considerably better than those of micron size. However, the aggregation of nanoparticles during cycling typically damages the performance at a very fast rate. Alloying Sn with several other metals, which are either active or inactive for lithium intercalation, is the second most effective approach for improving capacity retention. Binary Sn-based alloys, such as Sn–Cu [8–10], Sn–Ni [11–14], and Sn–Co [15–18], have been intensively studied. Several ternary Sn-based alloys were also considered for this purpose. For example, the Sn–Sb–Cu alloy synthesized via reductive co-precipitation by Wang et al. [19] was proven to be significantly better than binary Sn–Sb alloys in terms of cycling properties. Tabuchi et al. [20] designed a Sn_{75.4}Co_{18.1}Sb_{6.5} alloy and found that the alloy had a higher cycling capacity than Sn–Sb or Sn–Co binary alloys. The preparation of Sn-based materials with a novel

X.-J. Pang · C.-H. Tan · X.-H. Dai · X. Wang · G.-W. Qi ·
S.-Y. Zhang (✉)
School of Chemistry and Chemical Engineering, Shandong
University, Jinan 250100, China
e-mail: syzhang@sdu.edu.cn

S.-Y. Zhang
National Key Lab of Crystal, Shandong University,
Jinan 250100, China



Scheme 1 Methods of improving the capacity retention of Sn-based materials for lithium-ion battery applications

structure has been proven as another effective method to accommodate the large volume expansion [10, 14, 18, 21–25]. For example, Xue et al. [26] electrodeposited an Sn–Co alloy on a porous Cu film as the current collector. The result showed that the porous electrode performs better than the planar electrode because of the introduction of extra space to buffer the volume change. Scrosati and co-workers [12] designed a 3D Cu nanorod array by using a porous alumina membrane as template, and Sn–Ni alloy was then electrodeposited on the array. This 3D nanostructured Sn–Ni alloy electrode exhibited excellent capacity retention and high rate capability. Electrodissolution, which has been introduced by our group [10, 14, 18] to create controllable nanopores in the residual alloys, was found to be another effective method to improve both the capacity retention and rate performance of binary Sn-based alloys.

In the present work, post-electrodissolution treatment was performed on a ternary Sn–Sb–Co alloy film prepared via co-electroplating method. The structural feature and electrochemical performance change with electrodissolution treatment intervals were studied to optimize the preparation conditions for the Sn–Sb–Co alloys. Even though the porosity of the alloy after post-electrodissolution did not significantly increase, both the capacity retention and rate performance significantly improved.

2 Experimental

2.1 Preparation of Sn–Sb–Co alloy materials

An Sn–Sb–Co alloy film was electrodeposited on one side of a piece of Cu foil, which was 10 μm thick and was used as the current collector in LIBs. Prior to deposition, the Cu foil was washed with acetone and 0.1 mol L⁻¹ HCl to remove organic contaminants and oxides on the surface. Electrodeposition was conducted in a two-electrode, homemade electrolytic cell and the Cu foil loaded with Sn–

Sb–Co alloy film was used as the cathode and a 20 cm² Ti sheet as the anode. The composition of the electrodeposition bath is listed in Table 1. Electrodeposition was performed at a constant current density of 10 mA cm⁻² for 10 min at room temperature. The bath composition and operating conditions has been optimized experimentally. And it was found that, at this bath composition and operating conditions, an alloy Sn–Sb–Co film with compact structure and smooth surface could be obtained.

The electrodissolution treatment was performed in the same electrolytic cell with the as-deposited Sn–Sb–Co alloy on the Cu foil surface as the anode, an Ni net as the cathode, and a 0.1 mol L⁻¹ HCl solution as the electrolyte. Electrodissolution was conducted at different intervals, i.e., 4, 6, 8, 10, and 14 min at a constant current density of 5 mA cm⁻². The Sn–Sb–Co alloy samples were then washed with deionized water and absolute ethanol for three times and dried in a vacuum oven at 80 °C for 24 h. The samples were then cut into disks of the same size and weighed using an analytical balance with an accuracy of 0.1 mg to obtain the mass of the active material loaded on the Cu foil.

2.2 Structure characterization

The composition and morphology of the alloy samples were investigated using a JSM-7600F field emission scanning electron microscope (SEM, JEOL, Japan) equipped with an EDX detector at an accelerating voltage of 15 kV. A D8 Advance X-ray diffractometer (XRD, Bruker, Germany) was used to record the crystallographic information of the samples with Cu K α radiation at a scan rate of 0.5° s⁻¹. The specific surface area of the sample was measured using a Quadrasorb SI Surface area analyzer (Quantachrome, USA) based on the BET adsorption of N₂.

2.3 Cell assembling

CR2025 coin test cells were assembled in an Ar-filled glove box at room temperature. The Sn–Sb–Co alloy

Table 1 Bath composition for electrodeposition of the Sn–Sb–Co alloy

Chemicals	Concentration (g L ⁻¹)
SnCl ₂ ·2H ₂ O	28.2
SbCl ₃	3.25
CoCl ₂ ·6H ₂ O	3.0
K ₄ P ₂ O ₇ ·3H ₂ O	192.2
NaKC ₄ H ₄ O ₆ ·4H ₂ O	10.0
C ₂ H ₅ NO ₂	10.0
Gelatin	1.0

sample discs were used as the working electrode, and a lithium sheet was used as the counter and reference electrode. A total of 1 mol L⁻¹ LiPF₆ dissolved in an organic solvent mixture, which was composed of ethylene carbonate, dimethyl carbonate, and diethyl carbonate at a ratio of 1:1:1, was used as the electrolyte. A Celgard 2400 membrane was used to separate the working and counter electrodes.

2.4 Electrochemical characterization

The test cells were galvanostatically charged and discharged with a current density of 0.2 C rate on a CT2001C-001 Land battery test system (Jinnuo, Wuhan, China) at cut-off voltages between 0.05 and 1.5 V. The cyclic voltammograms of these samples were recorded using a CHI604A electrochemical work station (CH Instrument, Shanghai, China) within a voltage range of 0.0–2.0 V (vs. Li⁺/Li) at a scan rate of 0.5 mV s⁻¹. The rate performance of the sample was studied by charging and discharging the test cell at rates of 0.2, 1, 2, 5, and 10 C.

3 Results and discussion

3.1 Composition of the alloys

The XRD patterns of the Sn–Sb–Co alloys before and after electrodisolution treatment were recorded and are shown in Fig. 1. The strongest diffraction peaks related to the Cu foil substrate appeared at 2θ = 43.3° and 50.4° (JCPDS Card No. 04-0836, space group: Fm-3 m, 225). The diffraction peaks of the tetragonal Sn phase were at 2θ = 30.6°, 32.0°, 43.9°, 44.9°, 55.3°, 62.5°, 63.8°, and

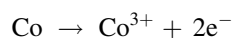
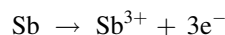
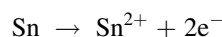
64.6° (JCPDS Card No. 04-0673, space group: I41/amd, 141). The peaks of the hexagonal Sn–Sb phase were at 2θ = 29.1°, 41.5°, 41.8°, 51.7°, 60.3°, 68.1°, and 68.5° (JCPDS Card No., 33-0118, space group: P-3 m, 166), whereas those of the tetragonal Sn–Co phase were at 2θ = 28.9°, 32.8°, 41.3°, 42.5°, 44.3°, and 52.2° [27]. The XRD patterns demonstrated that the Sn–Sb–Co alloy is composed of three distinct phases of Sn, Sn–Sb, and Sn–Co. When the electrodisolution time was increased, the diffraction peaks of the Sn phase weakened and were hard to see after 6 min of dissolution. This result suggests that the Sn phase dissolves considerably more rapidly than the accompanying Sn–Sb and Sn–Co phases. The surface composition of the alloys after electrodisolution treatment for different intervals was determined via EDX in area scan mode and is listed in Table 2.

As shown in Table 2, the Sn content in the residual alloys significantly decreased with increasing dissolution interval. This result is consistent with the XRD results. The increased molar ratio of Sb and Co in the residual alloys is the result of the rapid loss of the Sn phase.

3.2 Morphology of the samples

The color of the as-deposited Sn–Sb–Co alloy film was gray. After electrodisolution treatment, the film turned dark, which suggested the formation of small pores. The SEM images before and after electrodisolution treatment are shown in Fig. 2.

The as-deposited Sn–Sb–Co alloy film is composed of two parts: flat bottom and round aggregates embedded in the flat bottom. The round aggregates are composed of even smaller particles. During electrodisolution, the following reactions occur:



Due to electrodisolution of Sn, Sb and Co, these round aggregates became smaller, and numerous small pores were formed. Meanwhile, cracks formed and grew in the flat bottom during the treatment, which may be ascribed to

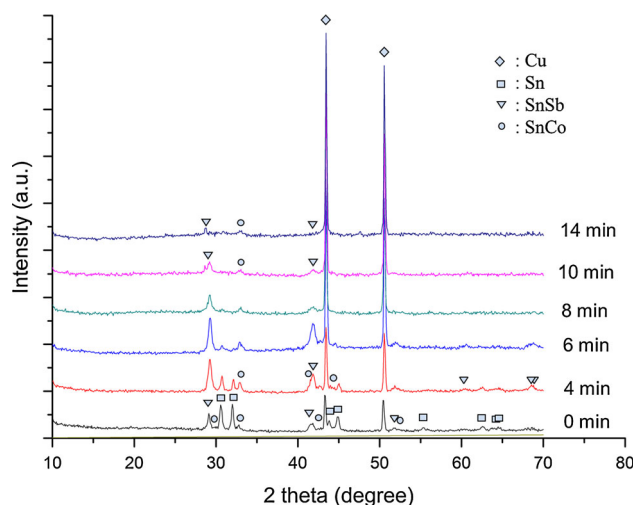


Fig. 1 XRD patterns of the Sn–Sb–Co alloy after electrodisolution for 0, 4, 6, 8, 10, and 14 min

Table 2 Surface composition of the Sn–Sb–Co alloys after electrodisolution treatment at different intervals

Elements	Molar ratio (%)					
	0 min	4 min	6 min	8 min	10 min	14 min
Sn	83.59	73.30	67.49	59.54	54.81	48.12
Sb	12.09	20.60	25.18	28.91	31.47	37.46
Co	4.32	6.10	7.32	11.55	13.72	14.42

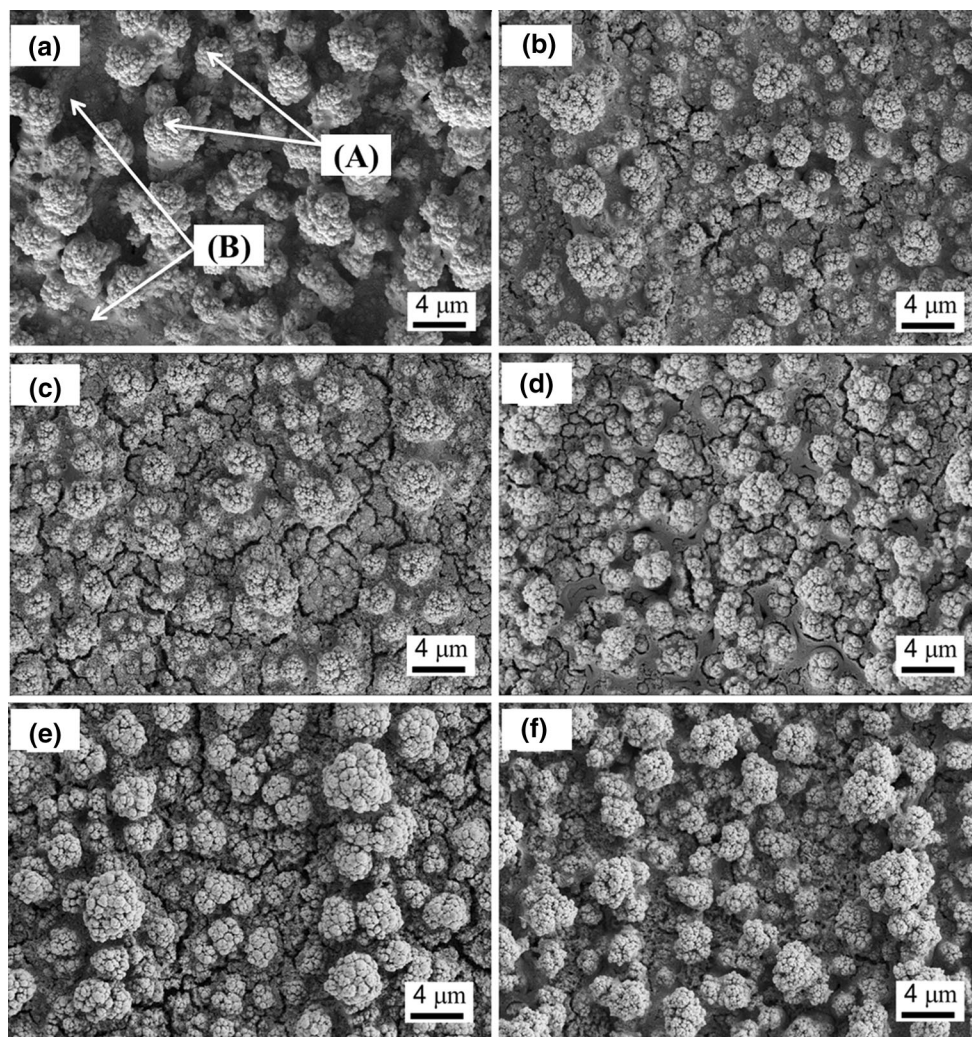


Fig. 2 SEM images of the Sn–Sb–Co alloys after electrodisso- lution treatment at different intervals: **a** 0, **b** 4, **c** 6, **d** 8, **e** 10, **f** 14 min, and the round aggregate (A) and the flat bottom (B)

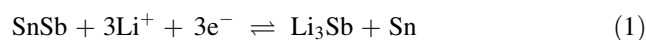
the residual tension inside the alloy and the rapid dissolution of the Sn phase. For the sample subjected to electrodisso- lution for 14 min, the cracks disappeared with the formation of micropores in the flat bottom.

3.3 Electrochemical performance

The cyclic voltammograms (CVs) of Sn–Sb–Co alloys before electrodisso- lution treatment and after 8 min of treatment are shown in Fig. 3.

The CV curves of the as-deposited Sn–Sb–Co alloy vary from those of the alloy after 8 min of electrodisso- lution treatment. For the as-deposited alloy, five reduction peaks marked with 1, 2, 3, 4, and 5, as well as their corresponding oxidation peaks 1', 2', 3', 4', and 5', can be observed. Peaks 1 and 1' correspond to the reversible lithiation of the Sn–Sb alloy, which forms Li_3Sb and Sn, as shown in (1).

Meanwhile, the other four peaks correspond to the lithia- tion reactions of Sn.



For the sample subjected to 8 min of electrodisso- lution treatment, only three pairs of peaks appeared. Peaks 1 and 1' correspond to the lithiation of the Sn–Sb alloy phase, and peaks 2–2' and 3–3' belong to a series of lithiation of Sn. Within 1.2–2.0 V, a distinct separation between the for- ward and reverse curves can be observed. This separation is due to the large double-layer capacitance, which suggests an increase in the specific surface area of the samples after electrodisso- lution treatment.

The charge and discharge curves of the as-deposited Sn–Sb–Co alloy and the sample after 8 min of electrodisso- lution treatment are shown in Fig. 4.

In Fig. 4a, four platforms appeared at 0.80, 0.65, 0.51, and 0.40 V in the discharge curves, which correspond to

Fig. 3 CVs of Sn–Sb–Co alloy before (a) and after 8 min of dissolution treatment (b)

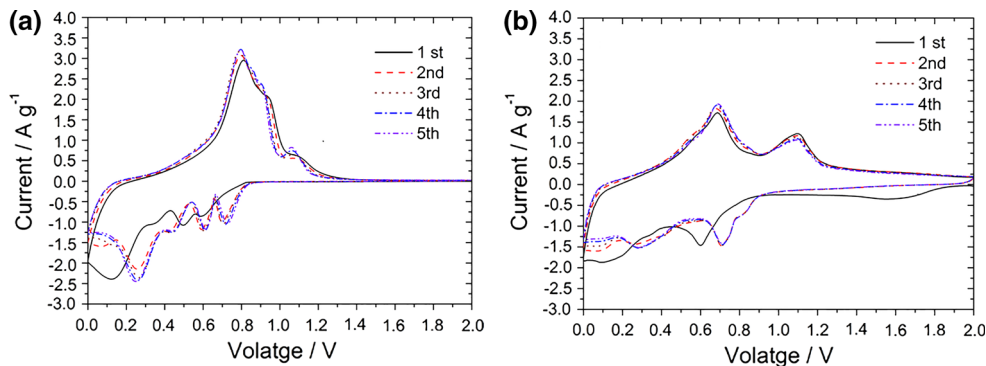
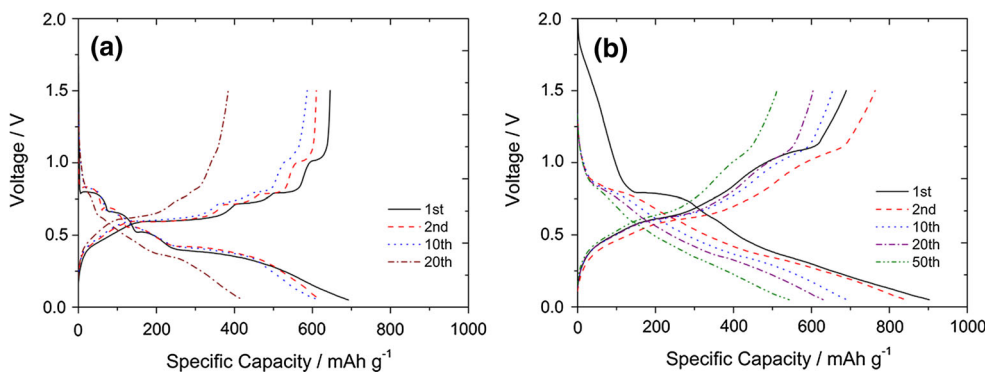


Fig. 4 Charge–discharge curves of the Sn–Sb–Co alloy before (a) and after 8 min of dissolution treatment (b)



the formation of Li_3Sb , Li_2Sn_5 , LiSn , and Li_7Sn_3 , respectively [28]. Four platforms at 0.60, 0.70, 0.77, and 1.20 V in the charge curves correspond to the formation of LiSn , Li_2Sn_5 , Sn, and Sb, respectively [28]. However, only one apparent platform at 0.80 V corresponding to Li–Sb formation and a less evident platform around 0.30 V, which correspond to a series of lithiation of Sn, could be seen in the discharge curves in Fig. 4b. In addition, two platforms at 0.75 and 1.10 V represent the lithiation of Sb and Sn, respectively. By comparing the charge and discharge curves, the lithiation potential of the Sb reaction does not significantly change, whereas the lithiation potential of Sn reactions significantly changes. This change can be attributed to the loss of the Sn phase as well as the reduced size of the Sn and Sn–Sb phases.

The initial discharge capacity of the as-deposited alloy electrode is 691 mAh g^{-1} , as shown in Fig. 5a. The specific capacity of the as-deposited alloy rapidly decayed after 13 cycles. This electrode completely lost its activity in 40 cycles, which is a marginally better performance than that of pure Sn electrode [29]. This result suggests that pulverization caused by the large volume change is still significant for the as-deposited Sn–Sb–Co ternary alloy. Therefore, the performance of the as-electrodeposited Sn–Sb–Co ternary alloy with only Sn as well as the separated Sn–Sb and Sn–Co binary alloy phases is worse than that reported and discussed in detail

in literature [20, 21]. Meanwhile, Fig. 5a also demonstrates the significant improvement in cycling performance with increasing electrodisolution treatment interval. The reversible capacity of the alloy after 10 min of electrodisolution treatment remained 580 mAh g^{-1} after 50 cycles. The capacity retention of this alloy sample after 50 cycles is 57 %, whereas that of the as-deposited Sn–Sb–Co alloy is only 5.5 % after 40 cycles. In Fig. 5b, the Coulombic efficiency of the initial cycle of the samples after electrodisolution treatment is considerably lower than that of the as-deposited sample, which indicates the large surface area of these samples. As such, more electricity is needed to reduce the surface oxide and form the solid electrolyte interface (SEI) membrane. The Coulombic efficiency also improves with increasing treatment interval. The Coulombic efficiency of the samples after treatment for 8, 10, and 14 min remains higher than 90 % for 50 cycles.

The rate performance of the sample was studied by a stepwise increase in the charge–discharge rate from 0.2 to 10 C and then returning back to 0.2 C, as shown in Fig. 6. For the as-deposited alloy, the capacity at a rate of 10 C is only 13.4 % of that at a rate of 0.2 C. The sample after 8 min of treatment delivers 624, 595, 534, 451, and 600 mAh g^{-1} at rates of 1, 2, 5, 10, and 0.2 C, respectively. The capacity of this sample at a rate of 10 C is 75 % of that at a rate of 0.2 C. Therefore, a significant

Fig. 5 Cycling performance of the Sn–Sb–Co alloys after treatment for different intervals: **a** discharge capacity, **b** Coulombic efficiency

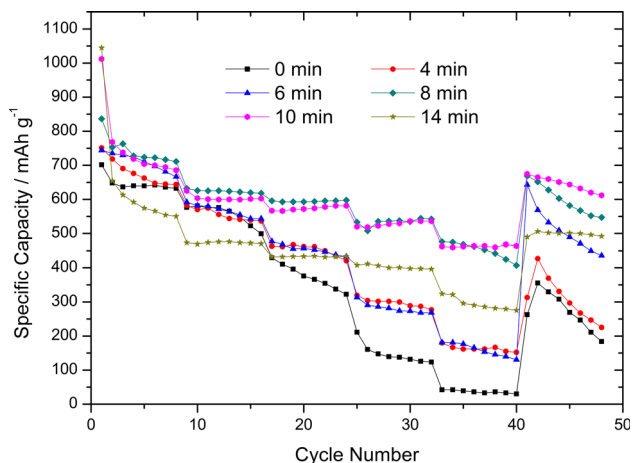
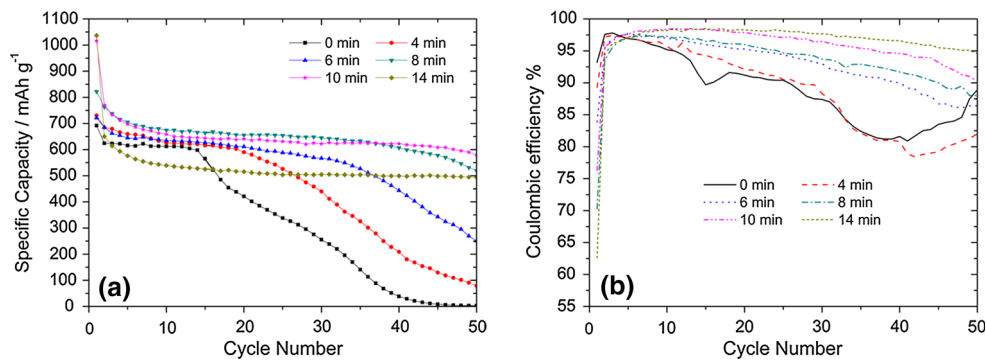


Fig. 6 Rate performance of the Sn–Sb–Co alloys after electrodisso- lution treatment at different intervals

improvement in rate performance can be observed by prolonging the electrodisso- lution treatment interval.

These results demonstrate that post-electrodisso- lution treatment is an effective method of improving the initial capacity, capacity retention, and rate performance of the electrodeposited Sn–Sb–Co alloys. The electrochemical performance of the alloys after more than 8 min of treatment is already close to those reported by Tabuchi [20] and Ke [21]. The easy preparation makes our procedure more advantageous. The improvement introduced by post-electrodisso- lution treatment is ascribed to the increased surface area as well as the reduced Sn content and particle size.

As shown in Fig. 2, more cracks and pores formed when the post treatment interval was prolonged, which resulted in increased surface area. The low initial charge–discharge Coulombic efficiency shown Fig. 5b and the separation of the charge and discharge curves shown in Fig. 3b both suggest the enlarged surface area. The specific area of the samples was measured via BET adsorption, as shown in Table 3.

The specific surface area of the as-deposited sample is $28.0 \text{ m}^2 \text{ g}^{-1}$. Prolonging the treatment interval increases the specific area accordingly. The larger specific surface

Table 3 Specific surface areas of the Sn–Sb–Co alloys after electrodisso- lution treatment at different intervals

Samples	BET surface area ($\text{m}^2 \text{ g}^{-1}$)
0 min	28.0
4 min	27.1
6 min	31.6
8 min	37.5
10 min	41.1
14 min	51.4

area improves the contact between alloy materials and the electrolyte, thereby increasing the active area, shortening the diffusion path of the lithium ion, and improving the electrochemical performance of the Sn–Sb–Co alloy. However, the increase in specific area is not as significant as the improvement in capacity retention, which suggests that the enlarged specific surface area is not the sole reason for the improvement. Therefore, the increased Sb and Co contents in the residual alloy were considered as the other reason accounting for the improvement in electrochemical performance.

As shown in Fig. 2a, the Sn–Sb–Co alloy sample is composed of two parts: the round aggregate, which is marked as (A), and the flat bottom, which is marked as (B). In Figs. 2b–d, the aggregates become smaller and more of the flat bottom is exposed as the electrodisso- lution treatment proceeds. Given that the current density at the aggregate part is higher than at the lower flat bottom, the rapid dissolution of the aggregate is expected. However, Figs. 2e, f show more aggregates. The emergence of more aggregates is attributed to the dissolution of the flat bottom part, which exposes the aggregates once embedded in the flat bottom. This process is illustrated by Scheme 2.

The composition of Part (A) after different treatment intervals was studied via EDX in spot scanning mode and is shown in Table 4. For the as-deposited Sn–Sb–Co alloy, no Co was found on the surface of Part (A). As electrodisso- lution proceeds, few Co are observed. This small amount of Co is attributed to the fact that at this stage, the

Scheme 2 Model for the composition and morphology changes caused by electrodisolution treatment

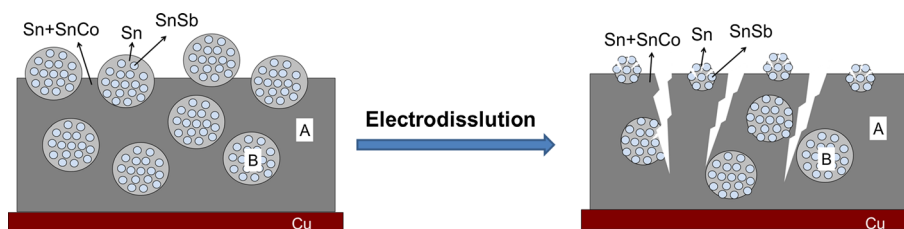
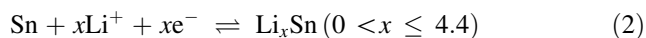


Table 4 Composition Part (A) at different treatment intervals

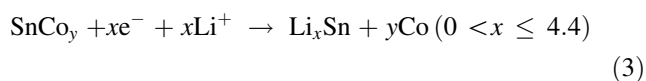
Elements	Molar ratio (%)		
	0 min	6 min	10 min
Sn	76.83	61.28	45.97
Sb	23.17	36.83	51.69
Co	0.00	1.89	2.34

size of the impact spot of the electron beam exceeds the size of the aggregate, and Co in the flat bottom part is collected. In the XRD image in Fig. 1, Part (A) consists of Sn and Sn–Sb phases, and Sn–Sb particles are wrapped in Sn [2]. As dissolution proceeds, Sn dissolves and exposes the Sn–Sb phase, which results in a decrease in Sn content and an increase in Sb content, as shown Table 4. Co exists homogeneously in Part B without distinct diffraction peaks.

The lithiation and delithiation occurred in two separated places, i.e., Part A and Part B. The lithiation and delithiation reactions in Part A can be indicated as Eqs. (1) and (2):



Meanwhile, the lithiation reactions in B can be written as Eq. (3):



When Eq. (1) occurs, Sn and Co buffer the volume change. When Eq. (3) occurs, Li_3Sb and Co buffer the volume changes. During delithiation, the atoms of Sn and Sb bond together and restore the original Sn–Sb phases [30–32]. The separation and restoration of the atoms could counteract the aggregation of Sn phase [3, 33, 34], which was one of the reasons for the rapid capacity decay. Unlike Sb, Co cannot be restored with Sn to form the Sn–Co alloy phase but instead forms nanosized particles after the first discharge [35]. The nanosized particles can prevent the pulverization of the alloy.

4 Conclusion

The as-electrodeposited Sn–Sb–Co alloy is composed of an Sn phase and two binary Sn–Sb and Sn–Co phases. The

Sn–Sb and Sn–Co alloy phases exist in different states: Sn–Sb forms a distinct alloy phase, whereas Co is distributed homogeneously in Sn. During electrochemical treatment, cracks and pores were formed because of the rapid dissolution of the Sn phase, which resulted in an increase in Sb and Co contents. The increased specific area, reduced particle size, and increased content of Sb and Co all contribute to higher initial capacity, improved capacity retention, and better rate performance. For the Sn–Sb–Co alloy after 10 min of dissolution treatment, the discharge capacity remained at 580 mAh g^{-1} after 50 cycles, which approximates that of materials synthesized via a more complicated metallurgical process. This result proves that the post-electrodisolution treatment is an effective method to improve the electrochemical performance of either binary or ternary Sn-based alloys.

Acknowledgments This work was financially supported by Natural Science Foundation of Shandong Province (Project No. ZR2009BM012), the 973 Project of China (No. 2011CB935901) and Open Project of State Key Laboratory of Crystal Material (KF1209).

References

1. Tarascon JM, Armand M (2001) Issues and challenges facing rechargeable lithium batteries. *Nature* 414:359–367
2. Winter M, Besenhard JO (1999) Electrochemical lithiation of tin and tin-based intermetallics and composites. *Electrochim Acta* 45:31–50
3. Courtney I, Dahn J (1997) Electrochemical and in situ X-ray diffraction studies of the reaction of lithium with tin oxide composites. *J Electrochem Soc* 144:2045–2052
4. Sivashanmugam A, Kumar TP, Renganathan NG, Gopukumar S, Wohlfahrt-Mehrens M, Garche J (2005) Electrochemical behavior of Sn/SnO₂ mixtures for use as anode in lithium rechargeable batteries. *J Power Sources* 144:197–203
5. Ui K, Kikuchi S, Kadoma Y, Kumagai N, Ito S (2008) Electrochemical characteristics of Sn film prepared by pulse electrodeposition method as negative electrode for lithium secondary batteries. *J Power Sources* 189:224–229
6. Huggins RA (1999) Lithium alloy negative electrodes. *J Power Sources* 81:13–19
7. Yu Y, Gu L, Wang C, Dhanabalan A, van Aken P, Maier J (2009) Encapsulation of Sn@carbon nanoparticles in bamboo-like hollow carbon nanofibers as an anode material in lithium-based batteries. *Angew Chem* 48:6485–6489
8. Kim MG, Sim S, Cho J (2010) Novel core-shell Sn–Cu anodes for lithium rechargeable batteries prepared by a redox-transmetalation reaction. *Adv Mater* 22:5154–5158

9. Ke FS, Huang L, Cai JS, Sun SG (2007) Electroplating synthesis and electrochemical properties of macroporous Sn–Cu alloy electrode for lithium-ion batteries. *Electrochim Acta* 52:6741–6747
10. Tan CH, Qi GW, Li YP, Guo J, Wang X, Kong DL, Wang HJ, Zhang SY (2012) Sn–Cu alloy materials with optimized nanoporous structure and enhanced performance for lithium-ion batteries prepared by dealloying. *Int J Electrochem Sci* 7:10303–10312
11. Mukaibo H, Sumi T, Yokoshima T, Momma T, Osaka T (2003) Electrodeposited Sn–Ni alloy film as a high capacity anode material for lithium-ion secondary batteries. *Electrochem Solid-State Lett* 6:A218–A220
12. Hassoun J, Panero S, Simon P, Taberna PL, Scrosati B (2007) High-rate, long-life Ni–Sn nanostructured electrodes for lithium-ion batteries. *Adv Mater* 19:1632–1635
13. Kotobuki M, Okada N, Kanamura K (2011) Design of a micro-pattern structure for a three dimensionally macroporous Sn–Ni alloy anode with high areal capacity. *Chem Commun* 47:6144–6146
14. Tan CH, Qi GW, Li YP, Guo J, Wang X, Kong DL, Wang HJ, Zhang SY (2013) The improved performance of porous Sn–Ni alloy as anode materials for lithium-ion battery prepared by electrochemical dissolution treatment. *Int J Electrochem Sci* 8:1966–1975
15. Ke FS, Huang L, Wei HB, Cai JS, Fan XY, Yang FZ, Sun SG (2007) Fabrication and properties of macroporous tin–cobalt alloy film electrodes for lithium-ion batteries. *J Power Sources* 170:450–455
16. Du ZJ, Zhang SC (2011) Enhanced electrochemical performance of Sn–Co nanoarchitected electrode for lithium ion batteries. *J Phys Chem C* 115:23603–23609
17. Tamura N, Fujimoto A, Kamino M, Fujitani S (2004) Mechanical stability of Sn–Co alloy anodes for lithium secondary batteries. *Electrochim Acta* 49:1949–1956
18. Tan CH, Qi GW, Li YP, Guo J, Wang X, Kong DL, Wang HJ, Zhang SY (2013) Performance enhancement of Sn–Co alloys for lithium-ion battery by electrochemical dissolution treatment. *J Alloy Compd* 574:206–211
19. Wang F, Zhao M, Song X (2008) Nano-sized SnSbCu_x alloy anodes prepared by co-precipitation for Li-ion batteries. *J Power Sources* 175:558–563
20. Tabuchi T, Hochgatterer N, Ogumi Z, Winter M (2009) Ternary Sn–Sb–Co alloy film as new negative electrode for lithium-ion cells. *J Power Sources* 188:552–557
21. Ke FS, Huang L, Solomon BC, Wei GZ, Xue LJ, Zhang B, Li JT, Zhou XD, Sun SG (2012) Three-dimensional nanoarchitecture of Sn–Sb–Co alloy as an anode of lithium-ion batteries with excellent lithium storage performance. *J Mater Chem* 22:17511–17517
22. Yu Y, Gu L, Lang XY, Zhu CB, Fujita T, Chen MW, Maier J (2011) Li Storage in 3D nanoporous Au-supported nanocrystalline tin. *Adv Mater* 23:2443–2447
23. Ke F, Huang L, Jiang H, Wei H, Yang F, Sun S (2007) Fabrication and properties of three-dimensional macroporous Sn–Ni alloy electrodes of high preferential (110) orientation for lithium ion batteries. *Electrochem Commun* 9:228–232
24. Fan XY, Ke FS, Wei GZ, Huang L, Sun SG (2009) Sn–Co alloy anode using porous Cu as current collector for lithium ion battery. *J Alloys Compd* 476:70–73
25. Kim R, Nam D, Kwon H (2010) Electrochemical performance of a tin electrode deposit with a multi-layered structure for Li-ion batteries. *J Power Sources* 195:5067–5070
26. Xue LJ, Xu YF, Huang L, Ke FS, He Y, Wang YX, Wei GZ, Li JT, Sun SG (2011) Lithium storage performance and interfacial processes of three dimensional porous Sn–Co alloy electrodes for lithium-ion batteries. *Electrochim Acta* 56:5979–5987
27. Goâmez E, Us EG, Ent JT, Alcobe X, Valleâs E (2001) Tin–cobalt electrodeposition from sulfate-gluconate baths. *J Appl Electrochem* 31:349–354
28. Hu RZ, Liu H, Zeng MQ, Liu JW, Zhu M (2012) Progress on Sn-based thin-film anode materials for lithium-ion batteries. *J Chin Sci Bull* 57:4119–4130
29. Morimoto H, Tobishima SI, Negishi H (2005) Anode behavior of electroplated rough surface Sn thin films for lithium-ion batteries. *J Power Sources* 146:469–472
30. Li H, Zhu GY, Huang XJ, Chen LQ (2000) Synthesis and electrochemical performance of dendrite-like nanosized SnSb alloy prepared by co-precipitation in alcohol solution at low temperature. *J Mater Chem* 10:693–696
31. Yang J, Winter M, Besenhard JO (1996) Small particle size multiphase Li-alloy anodes for lithium-ion batteries. *Solid State Ionics* 90:281–287
32. Besenhard JO, Yang J, Winter M (1997) Will advanced lithium-alloy anodes have a chance in lithium-ion batteries. *J Power Sources* 68:87–90
33. Courtney IA, McKinnon WR, Dahn JR (1999) On the aggregation of tin in SnO composite glasses caused by the reversible reaction with lithium. *J Electrochem Soc* 146:59–68
34. Courtney IA, Dahn JR (1997) Key factors controlling the reversibility of the reaction of lithium with SnO₂ and Sn₂BPO₆ glass. *J Electrochem Soc* 144:2943–2948
35. Ionica-Bousquet CM, Lippens PE, Aldon L, Olivier-Fourcade J, Jumas JC (2006) In situ ¹¹⁹Sn Mössbauer effect study of Li–CoSn₂ electrochemical system. *Chem Mater* 18:6442–6447